

Output Impedance Diffusion into Lossy Power Lines

Pooya Monshizadeh, Nima Monshizadeh, Claudio De Persis, and Arjan van der Schaft

Abstract—Output impedances are inherent elements of power sources in the electrical grids. In this paper, we give an answer to the following question: What is the effect of output impedances on the inductivity of the power network? To address this question, we propose a measure to evaluate the inductivity of a power grid, and we compute this measure for various types of output impedances. Following this computation, it turns out that network inductivity highly depends on the algebraic connectivity of the network. By exploiting the derived expressions of the proposed measure, one can tune the output impedances in order to enforce a desired level of inductivity on the power system. Furthermore, the results show that the more “connected” the network is, the more the output impedances diffuse into the network. Finally, using Kron reduction, we provide examples that demonstrate the utility and validity of the method.

Index Terms—Microgrid, Power network, Output impedance, Graph theory, Laplacian matrix, Kron reduction

I. INTRODUCTION

OUTPUT impedance is an important and inevitable element of any power producing device, such as synchronous generators and inverters. Synchronous generators typically possess a highly inductive output impedance according to their large stator coils, and are prevalently modeled by a voltage source behind an inductance. Similarly, inverters have an inductive output impedance due to the low pass filter in the output, which is necessary to eliminate the high frequencies of the modulation signal.

There are motives to add an impedance to the inherent output impedance of the inverters, one of the most important of which is to enhance the performance of droop controllers in a lossy network. Droop controllers show a better performance in a dominantly inductive network (or analogously in dominantly resistive networks for the case of inverse-droop controllers) [1]–[7] (see Figure 1). The additional output impedance is also employed to improve stability and correct the load sharing error [3], [8], [9], [10], supply harmonics to nonlinear loads [11], [2], [12], share current among sources resilient to parameters mismatch and synchronization error [13], decrease sensitivity to line impedance unbalances [4],

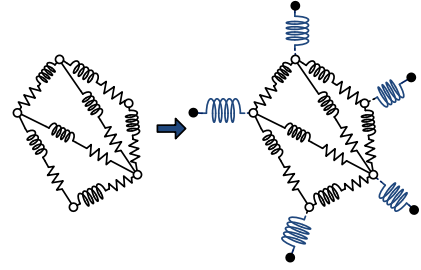


Fig. 1. Inductive outputs are typically added to the sources in order to assume inductive lines for the resulting network.

[14], [15], reduce the circulating currents [16], limit output current during voltage sags [17], minimize circulating power [18], and damp the LC resonance in the output filter [7]. In most of these methods, to avoid the costs and large size of an additional physical element, a *virtual output impedance* is employed, where the electrical behavior of a desired output impedance is simulated by the inverter controller block.

Although an inductive output impedance, either resulting from the inherent output filter or the added output impedance, is considered as a means to regulate the inductive behavior of the resulting network, there is a lack of theoretical analysis to verify the feasibility of this method and to quantify the effect of the output impedances on the network inductivity/resistivity. Note that the output impedance cannot be chosen arbitrarily large, since a large impedance substantially boosts the voltage sensitivity to current fluctuations, and results in high frequency noise amplification [7]. Furthermore, there is the fundamental challenge of quantifying inductivity/resistivity of a network, which is nontrivial unless the overall network has uniform line characteristics (homogeneous). This is not the case here as the augmented network will be nonuniform (heterogeneous) even if the initial network is.

In this paper, we examine the effect of the output impedances on a homogeneous power distribution grid by proposing a quantitative measure for the inductivity of the resulting heterogeneous network. Similarly, a dual measure is defined for its resistivity. Based on these measures, we show that the network topology plays a major role in the diffusion of the output impedance into the network. Furthermore, we exploit the proposed measures to maximize the effect of the added output impedances on the network inductivity/resistivity. We demonstrate the validity and practicality of the proposed method on various examples and special cases.

The structure of the paper is as follows: In Section II, the notions of Network Inductivity Ratio (Ψ_{NIR}) and Network Resistivity Ratio (Ψ_{NRR}) are proposed. In Section III, the

Pooya Monshizadeh and Arjan van der Schaft are with the Bernoulli Institute for Mathematics, Computer Science, and Artificial Intelligence, University of Groningen, 9700 AK, the Netherlands, p.monshizadeh@rug.nl, a.j.van.der.schaft@rug.nl

Nima Monshizadeh and Claudio De Persis are with the Engineering and Technology institute Groningen (ENTEG), University of Groningen, 9747 AG, the Netherlands, n.monshizadeh@rug.nl, c.de.persis@rug.nl

This work was supported by the STW perspective program “Robust Design of Cyber-physical Systems” under the auspices of the project “Energy Autonomous Smart Microgrids”.

proposed measures are analytically computed for various cases of output inductors and resistors. In Section IV the proposed measure is evaluated with the Kron reduction in the phasor domain. Finally, Section V is devoted to conclusions.

II. MEASURE DEFINITION

Consider an electrical network with an arbitrary topology, where we assume that all the sources and loads are connected to the grid via power converter devices (inverters) [19] (later in Section III, we show how to relax this assumption.). The network of this grid is represented by a connected and weighted undirected graph $\mathcal{G}(\mathcal{V}, \mathcal{E}, \Gamma)$. The nodes $\mathcal{V} = \{1, \dots, n\}$ represent the inverters, and the edge set \mathcal{E} accounts for the distribution lines. The total number of edges is denoted by m , i.e., $|\mathcal{E}| = m$. The edge weights are collected in the diagonal matrix Γ , and will be specified later.

For an undirected graph \mathcal{G} , the incidence matrix B is obtained by assigning an arbitrary orientation to the edges of \mathcal{G} and defining

$$b_{ik} = \begin{cases} +1 & \text{if } i \text{ is the tail of edge } k \\ -1 & \text{if } i \text{ is the head of edge } k \\ 0 & \text{otherwise} \end{cases}$$

with b_{ik} being the (i, k) th element of B .

We start our analysis with the voltages across the edges of the graph \mathcal{G} . We restrict this analysis to the low/medium voltage networks with short line lengths¹, where the shunt capacitance of the line (pi) model can be neglected [20, Ch.13], [21, App.1], [22, Ch.6]. Now let $R_e \in \mathbb{R}^{m \times m}$ and $L_e \in \mathbb{R}^{m \times m}$ be the diagonal matrices with the line resistances and inductances on their diagonal, respectively. We have

$$R_e I_e + L_e \dot{I}_e = B^\top V, \quad (1)$$

where $I_e \in \mathbb{R}^m$ denotes the current flowing through the edges. The orientation of the currents is taken in agreement with that of the incidence matrix. The vector $V \in \mathbb{R}^n$ indicates the voltages at the nodes. Let τ_k denote the physical distance between nodes i and j , for each edge $k \sim \{i, j\}$. We assume that the network is homogeneous, i.e. the distribution lines are made of the same material and possess the same resistance and inductance per length:

$$r = \frac{R_{e_k}}{\tau_{e_k}}, \quad l = \frac{L_{e_k}}{\tau_{e_k}}, \quad k = \{1, \dots, m\}.$$

Now, let the weight matrix Γ be specified as

$$\Gamma = \text{diag}(\gamma) := \text{diag}(\tau_1^{-1}, \tau_2^{-1}, \dots, \tau_m^{-1}). \quad (2)$$

We can rewrite (1) as [23]

$$rI_e + l\dot{I}_e = \Gamma B^\top V.$$

Hence, $rBI_e + lB\dot{I}_e = B\Gamma B^\top V$, and

$$rI + l\dot{I} = \mathcal{L}V, \quad (3)$$

where $I := BI_e$ is the vector of nodal current injections. The matrix $\mathcal{L} = B\Gamma B^\top$ is the Laplacian matrix of the graph $\mathcal{G}(\mathcal{V}, \mathcal{E}, \Gamma)$ with the weight matrix Γ .

Note that, as the network (3) is homogeneous, its inductivity behavior is simply determined by the ratio $\frac{l}{r}$. However, clearly, network homogeneity will be lost once the output impedances are augmented to the network. This makes the problem of determining network inductivity nontrivial and challenging. To cope with the heterogeneity resulting from the addition of the output impedances, we need to depart from the homogeneous form (3), and develop new means to assess the network inductivity. To this end, we consider the more general representation

$$RI + L\dot{I} = \mathcal{L}V_o, \quad (4)$$

where $V_o \in \mathbb{R}^n$ is the vector of voltages of the augmented nodes (black nodes in Figure 1), and $R \in \mathbb{R}^{n \times n}$ and $L \in \mathbb{R}^{n \times n}$ are matrices associated closely with the resistances and inductances of the lines, respectively. We will show that the overall network after the addition of the output impedances, can be described by (4). Note that this description cannot necessarily be realized with passive RL elements. Therefore, while the inductivity behavior of the homogeneous network (3) is simply determined by the ratio $\frac{l}{r}$, the one of (4) cannot be trivially quantified.

The idea here is to promote the rate of convergence as a suitable metric quantifying the inductivity/resistivity of the network. For the network dynamics in (3), the rate of convergence of the solutions is determined by the ratio $\frac{r}{l}$. The more inductive the lines are, the slower the rate of convergence is. Now, we seek for a similar property in (4). Notice that the solutions of (3) are damped with corresponding eigenvalues of $L^{-1}R$. Throughout the paper, we assume the following property:

Assumption 1 The eigenvalues of the matrix $L^{-1}R$ are all positive and real.

It will be shown that Assumption 1 is satisfied for all the cases considered in this paper.

Figure 2 sketches the behavior of homogeneous solutions of (4). Among all the solutions, we choose the fastest one as our measure for inductivity, and the slowest one for resistivity of the network. Opting for these worst case scenarios allows us to guarantee a prescribed inductivity or resistivity ratio by proper design of output impedances. These choices are formalized in the following definitions.

Definition 1 Let $I(t, I_0)$ denote the homogeneous solution of (4) for an initial condition $I_0 \in \text{im } B$. Let the set $M_L \subseteq \mathbb{R}^+$ be given by

$$M_L := \{\sigma \in \mathbb{R}^+ \mid \exists \mu \text{ s.t.} \\ \|I(t, I_0)\| \geq \mu e^{-\sigma t} \|I_0\|, \forall t \in \mathbb{R}^+, \forall I_0 \in \text{im } B\}.$$

Then we define the *Network Inductivity Ratio* (NIR) as

$$\Psi_{\text{NIR}} := \frac{1}{\inf(M_L)}.$$

¹A power line is defined as a short-length line if its length is less than 80 km [20].

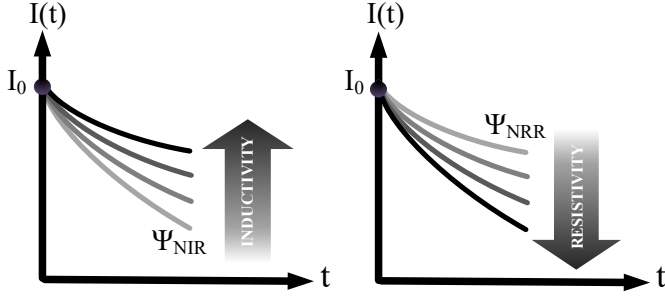


Fig. 2. Worst cases are selected for inductivity and resistivity measures.

Definition 2 Let $I(t, I_0)$ denote the homogeneous solution of (4) for an initial condition $I_0 \in \text{im } B$. Let the set $M_R \subseteq \mathbb{R}^+$ be given by

$$M_R := \{\sigma \in \mathbb{R}^+ \mid \exists \mu \text{ s.t.} \\ \|I(t, I_0)\| \leq \mu e^{-\sigma t} \|I_0\|, \forall t \in \mathbb{R}^+, \forall I_0 \in \text{im } B\}.$$

We define the *Network Resistivity Ratio* (NRR) as

$$\Psi_{\text{NRR}} := \sup(M_R).$$

□

Note that the set M_L is bounded from below and M_R is bounded from above by definition and Assumption 1. Interestingly, in case of the homogeneous network (3), i.e. without output impedances, we have $\Psi_{\text{NIR}} = \frac{\ell}{r}$ and $\Psi_{\text{NRR}} = \frac{r}{\ell}$, which are natural measures to reflect the inductivity and resistivity of an RL homogeneous network.

III. CALCULATING THE NETWORK

INDUCTIVITY/RESISTIVITY MEASURE ($\Psi_{\text{NIR}}/\Psi_{\text{NRR}}$)

In this section, based on Definitions 1 and 2, we compute the network inductivity/resistivity ratio for both cases of uniform and nonuniform output impedances.

A. Uniform Output Impedances

In most cases of practical interest, the output impedance consists of both inductive and resistive elements. We investigate the effect of the addition of such output impedances on the network inductivity ratio. The change in network resistivity ratio can be studied similarly, and thus is omitted here. Consider the uniform output impedances with the inductive part ℓ_o and the resistive component r_o (in series), added to the network (3). Note that the injected currents I now pass through the output impedances, as shown in Figure 3. Clearly, we have

$$V = V_o - r_o I - \ell_o \dot{I}. \quad (5)$$

Having (3) and (5), the overall network can be described as

$$(r_o \mathcal{L} + r \mathcal{I})I + (\ell_o \mathcal{L} + \ell \mathcal{I})\dot{I} = \mathcal{L}V_o, \quad (6)$$

where $\mathcal{I} \in \mathbb{R}^{n \times n}$ denotes the identity matrix, and \mathcal{L} is the Laplacian matrix of \mathcal{G} as before. In view of equation (4), the matrices R and L are given by $R = r_o \mathcal{L} + r \mathcal{I}$ and $L = \ell_o \mathcal{L} + \ell \mathcal{I}$, respectively. As both matrices are positive definite, the

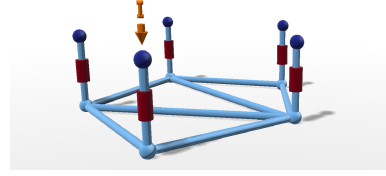


Fig. 3. The injected currents at the nodes of the original graph pass through the added output impedance.

eigenvalues of the product $L^{-1}R$ are all positive and real, see [24, Ch. 7]. Hence, Assumption 1 is satisfied. To calculate the measure Ψ_{NIR} for the inductivity of the resulting network, we investigate the convergence rates of the homogeneous solution of (6). This brings us to the following theorem:

Theorem 1 Consider a homogeneous network (3) with the resistance per length unit r and inductance per length unit ℓ . Suppose that an output resistance r_o and an output inductance ℓ_o are attached in series to each node. Assume that $\frac{r_o}{\ell_o} < \frac{r}{\ell}$. Then the network inductivity ratio is given by

$$\Psi_{\text{NIR}} = \frac{\ell_o \lambda_2 + \ell}{r_o \lambda_2 + r}, \quad (7)$$

where λ_2 is the algebraic connectivity² of the graph $\mathcal{G}(\mathcal{V}, \mathcal{E}, \Gamma)$.

Proof: The homogeneous solution is

$$I(t) = e^{-(r_o \mathcal{L} + r \mathcal{I})(\ell_o \mathcal{L} + \ell \mathcal{I})^{-1} t} I_0.$$

The Laplacian matrix can be decomposed as $\mathcal{L} = \mathcal{U}^\top \Lambda \mathcal{U}$. Here, \mathcal{U} is the matrix of eigenvectors and $\Lambda = \text{diag}\{\lambda_1, \lambda_2, \dots, \lambda_n\}$ where $\lambda_1 < \lambda_2 < \dots < \lambda_n$ are the eigenvalues of the matrix \mathcal{L} . Note that $\lambda_1 = 0$. We have

$$I(t) = e^{-\mathcal{U}(r_o \Lambda + r \mathcal{I})\mathcal{U}^\top (\mathcal{U}(\ell_o \Lambda + \ell \mathcal{I})\mathcal{U}^\top)^{-1} t} I_0 \\ = \mathcal{U} e^{-(r_o \Lambda + r \mathcal{I})(\ell_o \Lambda + \ell \mathcal{I})^{-1} t} \mathcal{U}^\top I_0 \\ = \left[\frac{1}{\sqrt{n}} \mathbb{1} \quad \tilde{\mathcal{U}} \right] e^{-\begin{bmatrix} \frac{r}{\ell} & 0 \\ 0_{(n-1) \times 1} & \tilde{\Lambda} \end{bmatrix} t} \begin{bmatrix} \frac{1}{\sqrt{n}} \mathbb{1}^\top \\ \tilde{\mathcal{U}}^\top \end{bmatrix} I_0,$$

where $\tilde{\Lambda} = \text{diag}\{\frac{r_o \lambda_2 + r}{\ell_o \lambda_2 + \ell}, \dots, \frac{r_o \lambda_n + r}{\ell_o \lambda_n + \ell}\}$. Noting that \mathcal{U} is unitary and by the Kirchhoff Law, $\mathbb{1}^\top I_0 = 0$, we have

$$I(t) = \tilde{\mathcal{U}} e^{-\tilde{\Lambda} t} \tilde{\mathcal{U}}^\top I_0 = \left(\sum_{i=1}^{n-1} e^{-\tilde{\lambda}_i t} \tilde{\mathcal{U}}_i \tilde{\mathcal{U}}_i^\top \right) \left(\sum_{i=1}^{n-1} \alpha_i \tilde{\mathcal{U}}_i \right) \\ = \sum_{i=1}^{n-1} \alpha_i e^{-\tilde{\lambda}_i t} \tilde{\mathcal{U}}_i,$$

where $\tilde{\mathcal{U}}_i$ denotes the i th column of $\tilde{\mathcal{U}}$, and we used again $\mathbb{1}^\top I_0 = 0$ to write I_0 as the linear combination

$$I_0 = \sum_{i=1}^{n-1} \alpha_i \tilde{\mathcal{U}}_i.$$

²The algebraic connectivity of either a directed or an undirected graph \mathcal{G} is defined as the second smallest eigenvalue of the Laplacian matrix throughout the paper. Note that the smallest eigenvalue is 0.

Hence

$$\|I(t)\|^2 = \sum_{i=1}^{n-1} \alpha_i^2 e^{-2\tilde{\lambda}_i t}. \quad (8)$$

Having $\frac{r_o}{\ell_o} < \frac{r}{\ell}$, it is straightforward to see that

$$\frac{r_o \lambda_2 + r}{\ell_o \lambda_2 + \ell} \geq \frac{r_o \lambda_i + r}{\ell_o \lambda_i + \ell}, \quad \forall i.$$

and bearing in mind that $\|I_0\|^2 = \sum_{i=1}^{n-1} \alpha_i^2$, we conclude that

$$\|I(t)\| \geq e^{-\frac{r_o \lambda_2 + r}{\ell_o \lambda_2 + \ell} t} \|I_0\|, \quad (9)$$

which yields $\Psi_{\text{NIR}} = \frac{\ell_o \lambda_2 + \ell}{r_o \lambda_2 + r}$. Note that (9) holds with equality in case I_0 belongs to the span of the corresponding eigenvector of the second smallest eigenvalue of the Laplacian matrix \mathcal{L} . This completes the proof. ■

Theorem 1 provides a compact and easily computable expression which quantifies the network inductivity behavior. Moreover, the expression (7) is an easy-to-use measure that can be exploited to choose the output impedances in order to impose a desired degree of inductivity on the network. The only information required is the line parameters r , and ℓ , and the algebraic connectivity of the network.

Algebraic connectivity is a measure of connectivity of the weighted graph \mathcal{G} , which depends on both the density of the edges and the weights (inverse of the lines lengths). Hence, Theorem 1 reveals the fact that: “*The more connected the network is, the more the output impedance diffuses into the network.*”.

The algebraic connectivity of the network can be estimated through distributed methods [25], [26]. Furthermore, line parameters (resistance and inductance) can be identified through PMUs (Phase Measurement Units) [27] [28] [29]. Therefore, our proposed measure can be calculated in a distributed manner.

Remark 1 In case the resistance part of the output impedance is negligible, i.e $r_o = 0$, the network inductivity ratio reduces to

$$\Psi_{\text{NIR}} = \frac{\ell_o \lambda_2 + \ell}{r},$$

In case $\frac{r_o}{\ell_o} > \frac{r}{\ell}$, the network inductivity ratio will be given by

$$\Psi_{\text{NIR}} = \frac{\ell_o \lambda_{\max} + \ell}{r_o \lambda_{\max} + r},$$

where λ_{\max} is the largest eigenvalue of the Laplacian matrix of \mathcal{G} . Furthermore, if $\frac{r_o}{\ell_o} = \frac{r}{\ell}$, then $\tilde{\Lambda} = \frac{r}{\ell} \mathcal{I}$ and $\Psi_{\text{NIR}} = \frac{r}{\ell}$. However, the condition $\frac{r_o}{\ell_o} < \frac{r}{\ell}$ assumed in Theorem 1 is more relevant since the resistance r_o of the inductive output impedance is typically small. □

As mentioned in Section I, in low-voltage microgrids where the lines are dominantly resistive, the inverse-droop method is employed. In this case, a purely resistive output impedance is of advantage [30].

Corollary 1 Consider a homogeneous distribution network with the resistance per length unit r , inductance per length

unit ℓ , and output inductors ℓ_o . Then the network resistivity ratio is given by

$$\Psi_{\text{NRR}} = \frac{r_o \lambda_2 + r}{\ell},$$

where λ_2 is the algebraic connectivity of the graph $\mathcal{G}(\mathcal{V}, \mathcal{E}, \Gamma)$.

Proof: The proof can be constructed in an analogous way to the proof of Theorem 1 and is therefore omitted. ■

Remark 2 The homogeneity assumption is ubiquitous in the literature of power network analysis (see e.g. [23], [31]–[36]). Here we show briefly how the results can be extended to the case of a heterogeneous network.

Using (1) and (5) together with $I = BI_e$ we have

$$R_e I_e + L_e \dot{I}_e = B^\top (V_o - r_o I - \ell_o \dot{I}) \quad (10)$$

$$(r_o \mathcal{L}_e + R_e) I_e + (\ell_o \mathcal{L}_e + L_e) \dot{I}_e = B^\top V_o, \quad (11)$$

where $\mathcal{L}_e := B^\top B$ is the *edge Laplacian*. Note that since the edge Laplacian is symmetric and positive semi-definite, the matrix $(\ell_o \mathcal{L}_e + L_e)^{-1} (r_o \mathcal{L}_e + R_e)$ has positive real eigenvalues, and hence analogously to the Definition 1 and Theorem 1, the network inductivity ratio can be defined and computed for the case of a heterogeneous network with additional output impedances. However, computing closed-form expressions for the proposed inductivity metric will become more challenging, and is not pursued in this work. □

Remark 3 One of the main desired features in microgrids is plug-and-play capability for planning and connection of the new sources. In most cases, a new node connects to the network initially through few edges. This results in a decrease in the algebraic connectivity of the overall network, e.g., as shown in [37], adding a pendant vertex and edge to a graph does not increase the algebraic connectivity. Therefore, for plug-and-play capability, larger output impedances should be employed in the network to compensate the possible drop in the algebraic connectivity, and thus the network inductivity ratio, resulting from attaching new nodes to the network. In some special cases, such as uniform line lengths, the additional required output impedances can be estimated using lower bounds on the algebraic connectivity; see [38] and [39] for more details on algebraic connectivity and its lower and upper bounds in various graphs. □

1) Case Study: Identical Line Lengths

Recall that the notion of network inductivity ratio allows us to quantify the inductivity behavior of the network, while the model (6), in general, cannot be synthesized with RL elements only. A notable special case where the model (6) can be realized with RL elements is a complete graph with identical line lengths. Although such case is improbable in practice, it provides an example to assess the validity and credibility of the introduced measures. Interestingly, Ψ_{NIR} matches precisely the inductance to resistance ratio of the lines of the synthesized network in this case:

Theorem 2 Consider a network with a uniform complete graph where all the edges have the length τ . Suppose that the lines have inductance $\ell_e \in \mathbb{R}$ and resistance $r_e \in \mathbb{R}$. Attach an output inductance ℓ_o in series with a resistance r_o to each node. Then the model of the augmented graph can be equivalently synthesized by a new RL network with identical lines, each with inductance $\ell_c := n\ell_o + \ell_e$ and resistance $r_c := nr_o + r_e$, where n denotes the number of nodes. Furthermore, the resulting network inductivity ratio Ψ_{NIR} is equal to $\frac{\ell_c}{r_c}$.

Proof: The nodal injected currents satisfy $rI + \ell\dot{I} = \mathcal{L}V$. In this network, $r = \frac{r_e}{\tau}$, $\ell = \frac{\ell_e}{\tau}$, and $\mathcal{L} = \frac{n}{\tau}\Pi$ where $\Pi := \mathcal{I} - \frac{1}{n}\mathbf{1}\mathbf{1}^\top$. Hence,

$$r_e I + \ell_e \dot{I} = n\Pi V. \quad (12)$$

By appending the output impedance we have $V = V_o - r_o I - \ell_o \dot{I}$. Hence (12) modifies to

$$(nr_o\Pi + r_e\mathcal{I})I + (n\ell_o\Pi + \ell_e\mathcal{I})\dot{I} = n\Pi V_o,$$

which results in

$$(n\ell_o\Pi + \ell_e\mathcal{I})^{-1}(nr_o\Pi + r_e\mathcal{I})I + \dot{I} = n(n\ell_o\Pi + \ell_e\mathcal{I})^{-1}\Pi V_o.$$

Since $(n\ell_o\Pi + \ell_e\mathcal{I})^{-1} = \frac{1}{\ell_e + n\ell_o}\mathcal{I} + \frac{\ell_o}{\ell_e(\ell_e + n\ell_o)}\mathbf{1}\mathbf{1}^\top$, we obtain

$$(nr_o\Pi + r_e\mathcal{I})I + (n\ell_o + \ell_e)\dot{I} = n\Pi V_o, \quad (13)$$

where we used $\mathbf{1}^\top I = 0$ and $\mathbf{1}^\top \Pi = 0$. Similarly we have

$$I + \ell_c(nr_o\Pi + r_e\mathcal{I})^{-1}\dot{I} = n(nr_o\Pi + r_e\mathcal{I})^{-1}\Pi V_o,$$

and hence $r_c I + \ell_c \dot{I} = n\Pi V_o$. This equation is analogous to (12) and corresponds to a uniform complete graph with identical line resistance $r_c = nr_o + r_e$ and inductance $\ell_c = n\ell_o + \ell_e$.

Note that the algebraic connectivity of the weighted Laplacian \mathcal{L} is $\frac{n}{\tau}$. By Theorem 1, the inductivity ratio is then computed as

$$\Psi_{\text{NIR}} = \frac{\frac{n}{\tau}\ell_o + \ell}{\frac{n}{\tau}r_o + r} = \frac{\ell_c}{r_c}.$$

2) Case Study: Constant Current Loads

So far, we have considered loads which are connected via power converters. The same definitions and results can be extended to the case of loads modeled with constant current sinks. Consider the graph $\mathcal{G}(\mathcal{V}, \mathcal{E}, \Gamma)$ divided into source (S) and load nodes (L), and decompose the Laplacian matrix accordingly as

$$\mathcal{L} = \begin{bmatrix} \mathcal{L}_{SS} & \mathcal{L}_{SL} \\ \mathcal{L}_{LS} & \mathcal{L}_{LL} \end{bmatrix}.$$

We have

$$rI_S + \ell\dot{I}_S = \mathcal{L}_{SS}V_S + \mathcal{L}_{SL}V_L \quad (14)$$

$$rI_L + \ell\dot{I}_L = \mathcal{L}_{LS}V_S + \mathcal{L}_{LL}V_L. \quad (15)$$

Suppose that the load nodes are attached to constant current loads $I_L = -I_L^*$. Then from (15) we obtain

$$-rI_L^* = \mathcal{L}_{LS}V_S + \mathcal{L}_{LL}V_L,$$

and therefore

$$-r\mathcal{L}_{LL}^{-1}I_L^* - \mathcal{L}_{LL}^{-1}\mathcal{L}_{LS}V_S = V_L. \quad (16)$$

Substituting (16) into (14) yields

$$rI_S + \ell\dot{I}_S = \mathcal{L}_{\text{red}}V_S - r\mathcal{L}_{SL}\mathcal{L}_{LL}^{-1}I_L^*.$$

Here the Scur complement $\mathcal{L}_{\text{red}} = \mathcal{L}_{SS} - \mathcal{L}_{SL}\mathcal{L}_{LL}^{-1}\mathcal{L}_{LS}$ is again a Laplacian matrix known as the *Kron-reduced* Laplacian [40], [41]. Bearing in mind that $V_G = V_o - \ell_o\dot{I}_S - r_oI_S$, the system becomes

$$(r\mathcal{I} + r_o\mathcal{L}_{\text{red}})I_S + (\ell\mathcal{I} + \ell_o\mathcal{L}_{\text{red}})\dot{I}_S = \mathcal{L}_{\text{red}}V_o - r\mathcal{L}_{SL}\mathcal{L}_{LL}^{-1}I_L^*, \quad (17)$$

and one can repeat the same analysis as above working with \mathcal{L}_{red} instead of \mathcal{L} . Note that (17) matches the model (4) with the difference of a constant. As this constant term does not affect the homogeneous solution, the network inductivity and resistivity ratios are obtained analogously as before, where the algebraic connectivity is computed based on the Kron reduced Laplacian. \square

B. Non-uniform Output Impedances

In this section we investigate the case where output inductances with different magnitudes are connected to the network, and we quantify the network inductivity ratio Ψ_{NIR} under this non-uniform addition. The case with non-uniform resistances can be treated in an analogous manner.

For the sake of simplicity, throughout this subsection, we consider the case where the resistive parts of the output impedances are negligible (see Remark 4 for relaxing this assumption). Let $D = \text{diag}(\ell_{o_1}, \ell_{o_2}, \dots, \ell_{o_n})$, where ℓ_{o_i} is the (nonzero) output inductance connected to the node i . We have

$$rI + \ell\dot{I} = \mathcal{L}V, \quad V = V_o - D\dot{I},$$

and hence

$$rI + (\ell\mathcal{I} + \mathcal{L}D)\dot{I} = \mathcal{L}V_o. \quad (18)$$

Note that $\mathcal{L}D$ is similar to $D^{\frac{1}{2}}\mathcal{L}D^{\frac{1}{2}}$ and therefore has nonnegative real eigenvalues. In view of equation (4), here $R = r\mathcal{I}$ and $L = \ell\mathcal{I} + \mathcal{L}D$. Hence, the matrix $L^{-1}R$ possesses positive real eigenvalues, and Assumption 1 holds.

The matrix $\mathcal{L}D$ is also similar to $D\mathcal{L}$, which can be interpreted as the (asymmetric) Laplacian matrix of a directed connected graph noted by $\hat{\mathcal{G}}(\mathcal{V}, \hat{\mathcal{E}}, \hat{\Gamma})$ with the same nodes as the original graph $\mathcal{V} = \{1, \dots, n\}$, but with directed edges $\hat{\mathcal{E}} \subset \mathcal{V} \times \mathcal{V}$. As shown in Figure 4, in this representation, for any $(i, j) \in \hat{\mathcal{E}}$, there exists a directed edge from node i to node j with the weight $\ell_{o_i}\tau_{ij}^{-1}$ (recall that τ_{ij}^{-1} is the weight of the edge $\{i, j\} \in \mathcal{E}$ of the original graph \mathcal{G}). Hence, the weight matrix $\hat{\Gamma} \in \mathbb{R}^{2m \times 2m}$ is the diagonal matrix with the weights $\ell_{o_i}\tau_{ij}^{-1}$ on its diagonal. Note that the edge set $\hat{\mathcal{E}}$ is symmetric in the sense that $(i, j) \in \hat{\mathcal{E}} \Leftrightarrow (j, i) \in \hat{\mathcal{E}}$, and its cardinality is equal to $2m$. We take advantage of this graph to obtain the network inductivity ratio Ψ_{NIR} , as formalized in the following theorem.

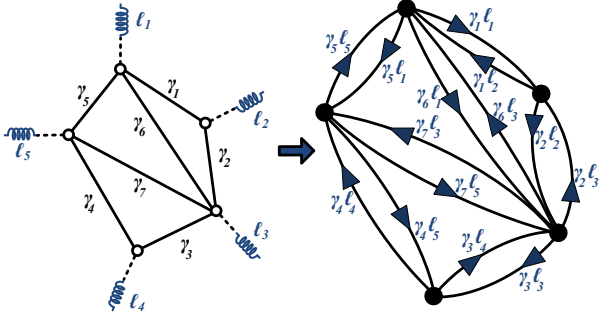


Fig. 4. Output inductances appear as weights in the corresponding directed graph, with the Laplacian $D\mathcal{L}$.

Theorem 3 Consider a homogeneous network with the resistance per length unit r , inductance per length unit ℓ , edge lengths τ_1, \dots, τ_n , and output inductors $\ell_{o_1}, \ell_{o_2}, \dots, \ell_{o_n}$. Then the network inductivity ratio is given by

$$\Psi_{\text{NIR}} = \frac{\lambda_2 + \ell}{r},$$

where λ_2 is the algebraic connectivity of the graph $\hat{\mathcal{G}}(\mathcal{V}, \hat{\mathcal{E}}, \hat{\Gamma})$ defined above.

Proof: Let $\mathcal{L}' = D^{\frac{1}{2}}\mathcal{L}D^{\frac{1}{2}}$. The homogeneous solution to (18) is

$$\begin{aligned} I(t) &= e^{-r(\ell\mathcal{I} + \mathcal{L}D)^{-1}t} I_0 \\ &= D^{-\frac{1}{2}} e^{-rD^{\frac{1}{2}}(\ell\mathcal{I} + \mathcal{L}D)^{-1}D^{-\frac{1}{2}}t} D^{\frac{1}{2}} I_0 \\ &= D^{-\frac{1}{2}} e^{-r(\ell\mathcal{I} + \mathcal{L}')^{-1}t} D^{\frac{1}{2}} I_0. \end{aligned}$$

Note that \mathcal{L}' is positive semi-definite and thus $\ell\mathcal{I} + \mathcal{L}'$ is invertible. Bearing in mind that 0 is an eigenvalue of the matrix \mathcal{L}' with the corresponding normalized eigenvector $\mathcal{U}_1 = (\mathbb{1}^\top D^{-1}\mathbb{1})^{-\frac{1}{2}} D^{-\frac{1}{2}}\mathbb{1}$, and by the spectral decomposition $\mathcal{L}' = \mathcal{U}\Lambda\mathcal{U}^\top$, we find that

$$\begin{aligned} I(t) &= D^{-\frac{1}{2}} e^{-r(\ell\mathcal{I} + \Lambda)\mathcal{U}^\top}^{-1} t D^{\frac{1}{2}} I_0 \\ &= D^{-\frac{1}{2}} \mathcal{U} e^{-r(\ell\mathcal{I} + \Lambda)^{-1}t} \mathcal{U}^\top D^{\frac{1}{2}} I_0 \\ &= D^{-\frac{1}{2}} \begin{bmatrix} \mathcal{U}_1 & \tilde{\mathcal{U}} \end{bmatrix} e^{-r \begin{bmatrix} \frac{1}{\ell} & 0 \\ 0 & (n-1) \times 1 \end{bmatrix} t} \tilde{\Lambda} \begin{bmatrix} \mathcal{U}_1^\top \\ \tilde{\mathcal{U}}^\top \end{bmatrix} D^{\frac{1}{2}} I_0, \end{aligned}$$

where $\tilde{\Lambda} = \text{diag}\{\frac{1}{\lambda_2 + \ell}, \frac{1}{\lambda_3 + \ell}, \dots, \frac{1}{\lambda_n + \ell}\}$ and $0 < \lambda_2 < \lambda_3 < \dots < \lambda_n$ are nonzero eigenvalues of the matrix \mathcal{L}' . Let $\tilde{I}(t) = D^{\frac{1}{2}} I(t)$. Noting that by the Kirchhoff Law, $\mathbb{1}^\top I_0 = 0$, we have

$$\tilde{I}(t) = \tilde{\mathcal{U}} e^{-r\tilde{\Lambda}t} \tilde{\mathcal{U}}^\top \tilde{I}_0.$$

Since $\mathcal{U}_1^\top \tilde{I}_0 = 0$ we can write \tilde{I}_0 as the linear combination $\tilde{I}_0 = \tilde{\mathcal{U}}X$, $X \in \mathbb{R}^{(n-1) \times 1}$. Now we have

$$\tilde{I}(t) = \tilde{\mathcal{U}} e^{-r\tilde{\Lambda}t} X, \quad \|\tilde{I}(t)\|^2 = X^\top e^{-2r\tilde{\Lambda}t} X.$$

Hence

$$\begin{aligned} \|\tilde{I}(t)\|^2 &\geq e^{-\frac{2r}{\lambda_2 + \ell}t} \|\tilde{I}_0\|^2, \\ I^\top(t) D I(t) &\geq e^{-\frac{2r}{\lambda_2 + \ell}t} I_0^\top D I_0, \\ \|I(t)\| &\geq \mu e^{-\frac{r}{\lambda_2 + \ell}t} \|I_0\|, \end{aligned}$$

where

$$\mu := \sqrt{\frac{\min_i(\ell_{o_i})}{\max_i(\ell_{o_i})}}.$$

This yields $\Psi_{\text{NIR}} = \frac{\lambda_2 + \ell}{r}$. Note that the eigenvalues of \mathcal{L}' and $D\mathcal{L}$ are the same. This completes the proof. ■

Remark 4 The results of Theorem 3 can be generalized to the case of non-uniform output impedances, each containing a nonzero resistor r_o and a nonzero inductor ℓ_o in series. In this case, the network can be modeled by

$$(r\mathcal{I} + \mathcal{L}D_r)I + (\ell\mathcal{I} + \mathcal{L}D_\ell)\dot{I} = \mathcal{L}V_o, \quad (19)$$

where $D_r := \text{diag}(r_{o_1}, r_{o_2}, \dots, r_{o_n})$ and $D_\ell := \text{diag}(\ell_{o_1}, \ell_{o_2}, \dots, \ell_{o_n})$. Analogously to the proof of Theorem 3, it can be shown that the network inductivity ratio is calculated as

$$\Psi_{\text{NIR}} = \min_{i \in \{2, 3, \dots, n\}} \frac{\lambda_{\ell_i} + \ell}{\lambda_{r_i} + r},$$

where λ_{ℓ_i} denotes the i th eigenvalue of the matrix $\mathcal{L}D_\ell$, and $\lambda_{\ell_1} = 0$. Similarly, λ_{r_i} denotes the i th eigenvalue of the matrix $\mathcal{L}D_r$, and $\lambda_{r_1} = 0$. □

Exploiting the results of [42], bearing in mind that \mathcal{L} and D are both positive semi-definite matrices, we have

$$\lambda_2(\mathcal{L}) \min_i \ell_{o_i} \leq \lambda_2(D\mathcal{L}) \leq \lambda_2(\mathcal{L}) \max_i \ell_{o_i}. \quad (20)$$

These bounds can be used to ensure that the network inductivity ratio lies within certain values, without explicitly calculating the algebraic connectivity of the directed graph associated with the Laplacian $D\mathcal{L}$.

Optimizing the network inductivity ratio: The results proposed can be also exploited to maximize the diffusion of output impedances into the network. This can be achieved by an optimal distribution of the inductors among the sources such that the network inductivity ratio is maximized. Below is an example illustrating this point on a network with a star topology. Another example using Kron reduction and phasors will be provided in Section IV.

Example 1 Consider the graph \mathcal{G} with the Laplacian \mathcal{L} , consisting of four nodes in a star topology. The line lengths are 5pu, 7pu, and 9pu, as depicted in Figure 5. Note that here again, the weights of the edges are the inverse of the distances. Attach the output impedances $D = \text{diag}\{\ell_{o_1}, \ell_{o_2}, \ell_{o_3}, \ell_{o_4}\}$ to each inverter, and assume that we have limited resources of inductors, namely ³

$$\sum_i \ell_{o_i} = c, \quad c \in \mathbb{R}^+. \quad (21)$$

Figure 5 shows different values of the second smallest eigenvalue of the matrix $D\mathcal{L}$. We obtain that the maximal algebraic connectivity is achieved when no output impedance is used (wasted) for the node in the middle. Interestingly, the optimal

³Note that the budget constraint (21) can also be used to reflect any disadvantage resulting from a large output impedance, e.g. the voltage drop.

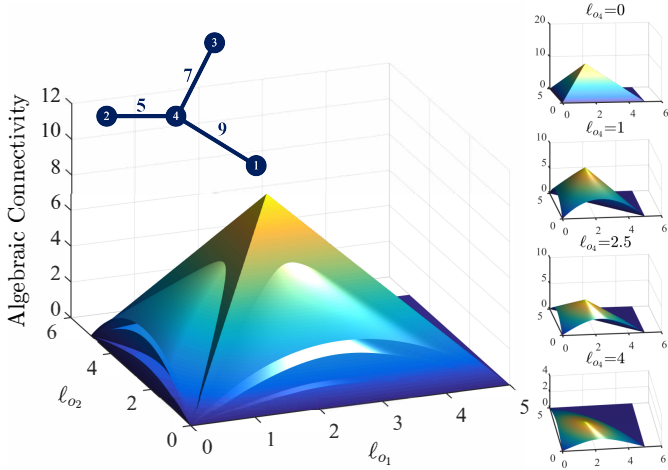


Fig. 5. Algebraic connectivity of the directed graph associated with the Laplacian $D\mathcal{L}$, where \mathcal{L} is the Laplacian of the star graph shown in top left corner. The budget constraint is $\sum_i \ell_{o_i} = c = 5\text{mH}$. On the right, the algebraic connectivity is plotted as a function of ℓ_{o_1} and ℓ_{o_2} for different values of ℓ_{o_i} . Note that $\ell_{o_3} = c - \ell_{o_1} - \ell_{o_2} - \ell_{o_4}$. On the left, all the four subplots are merged. Clearly, the optimal algebraic connectivity is achieved where no output impedance is used for node 4 (the middle node), and $\ell_{o_1} = 2.20\text{mH}$, $\ell_{o_2} = 1.23\text{mH}$, $\ell_{o_3} = 1.57\text{mH}$ are used for nodes 1, 2, and 3 respectively.

TABLE I
SIMULATION PARAMETERS

	Load ₁	Load ₂	Load ₃	Source
Measurement Delay (ms)	6	6	5	8
Droop Coefficient (pu)	0.07	0.14	0.14	0.28
Distance from the Source (m)	90	50	70	-
Voltage (pu)	1.05	1.10	0.95	0.96
Nominal Active Power (pu)	-0.9	-0.8	-1.2	1.5

value of output inductor for each node is proportional to its distance to the middle node.

Next we compare the performance of the droop controlled inverters in two different cases: i) the network with the optimized output impedances as above, and ii) the network with evenly distributed output impedances. To this end, suppose that a source is connected to the middle node (node 4 in Figure 5), and three constant power loads are connected to the outer nodes (nodes 1, 2, and 3 in Figure 5) via droop-controlled power converters with the parameters given by Table 1. Here, all the distribution lines are assumed to have the same reactance per length equal to $\omega\ell = 1.0 \frac{\Omega}{\text{km}}$ and resistance per length equal to $r = 0.1 \frac{\Omega}{\text{km}}$. At time $t = 0$, the loads are increased with 10% of their nominal value. The frequency of the inverters are shown in Figure 6. It is evident that the droop controllers perform better in the network with the optimized network inductivity ratio Ψ_{NIR} (top), compared to the case of evenly distributed output inductances (below), where the solutions fail to converge. \square

The results of this subsection for non-uniform output impedances allow for the analysis of the networks containing non-tunable output impedances, e.g. constant impedance loads

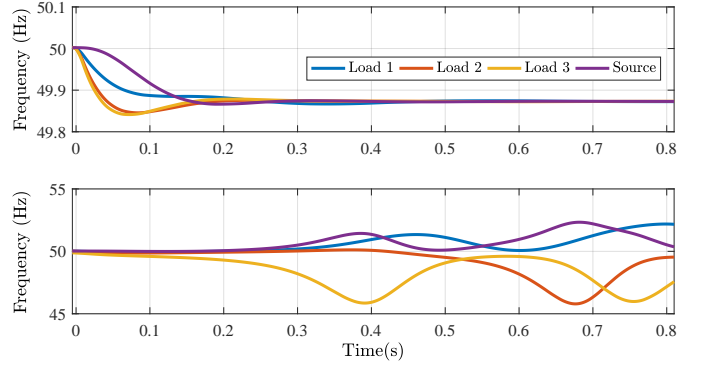


Fig. 6. Comparison of droop controllers performance between the network with the optimized Ψ_{NIR} (top), and a network with evenly distributed output inductances (below).

and synchronous generators/motors which can be modeled as a voltage source/sink behind a reactance. The optimization (and maximization of the algebraic connectivity) in this case involves only tuning the diagonal elements of the matrices D_r and D_l in (19) associated with the tunable output impedances.

IV. KRON REDUCTION IN PHASOR DOMAIN AND THE NETWORK INDUCTIVITY RATIO

By leveraging Kron reduction and using the phasor domain, it is sometimes possible to synthesize an RL circuit for the augmented network model (4) (see [43] for more details). As depicted in Figure 7, in the Kron reduced graph some of the edges coincide with the lines of the original network into which the output impedances were diffused, while others (dotted line) are created as a result of the Kron reduction. We refer to the former as *physical* and to the latter as *virtual* lines. To derive the Kron-reduced model, we first write the nodal currents as

$$\begin{bmatrix} I \\ 0 \end{bmatrix} = \begin{bmatrix} y_o \mathcal{I} & -y_o \mathcal{I} \\ -y_o \mathcal{I} & y_o \mathcal{I} + y_\ell \mathcal{L} \end{bmatrix} \begin{bmatrix} V_o \\ V \end{bmatrix},$$

where

$$y_o = \frac{1}{j\omega\ell_o}, \quad y_\ell = \frac{1}{r + j\omega\ell}.$$

The Kron-reduced model is then obtained as

$$\mathcal{Y}_{\text{red}} = y_o \left[\mathcal{I} - \left(\mathcal{I} + \frac{y_\ell}{y_o} \mathcal{L} \right)^{-1} \right]. \quad (22)$$

Since every path between the outer nodes of the graph passes only through internal nodes (see Figure 7), the resulting Kron-reduced network is a complete graph [44]. In the following example, we compare the line phase angles

$$\theta_{ij} := \arctan \frac{\text{Im}(1/\mathcal{Y}_{\text{red}ij})}{\text{Re}(1/\mathcal{Y}_{\text{red}ij})}$$

for the line $\{i, j\}$, to the phase angles suggested by Ψ_{NIR} , namely

$$\theta_{\text{NIR}} := \arctan(\omega\Psi_{\text{NIR}}). \quad (23)$$

Note that the term ω in the above is included to obtain reactance to resistance ratio from inductance to resistance ratio.

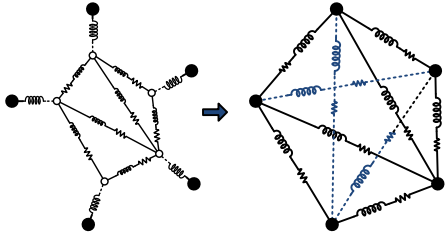


Fig. 7. Kron reduction of an arbitrary graph with added output impedances.

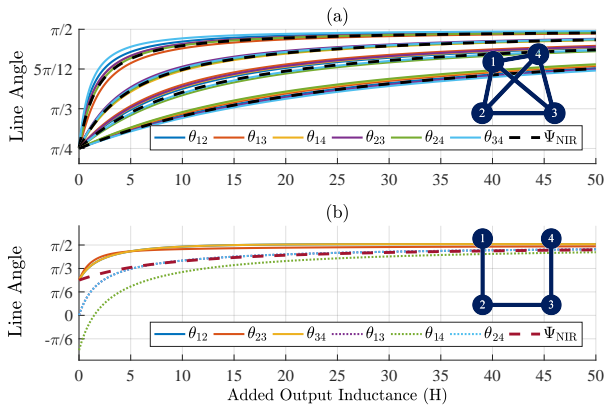


Fig. 8. (a) Complete graph. The initial phase angle of the lines is $\frac{\pi}{4}$ and the line lengths are the following 4 cases (from top to bottom): $[\tau_{12}, \tau_{13}, \tau_{14}, \tau_{23}, \tau_{24}, \tau_{34}] = [5, 6, 9, 7, 4, 6]$; $[20, 19, 20, 21, 20, 22]$; $[40, 37, 35, 49, 46, 38]$; $[100, 105, 93, 87, 110, 89]$; (b) Path graph. Virtual lines are shown by dots. The initial phase angle of the lines is $\frac{\pi}{4}$ and the line lengths are equal to 5.

Example 2 *Line angles of a Kron-reduced Graph with uniform output impedances.*

(a) Consider a 4-node complete graph with different distribution line lengths. As shown in Figure 8a, the proposed measure matches with the overall behavior of the line angles as the added output inductance increases. (b) Consider a 4-node uniform path graph. Figure 8b shows that the least inductivity behavior is observed for the virtual lines. Hence the less virtual lines the reduced graph contains, the more output impedance diffuses in the network, which is consistent with our results in Section III. Also note that the inductance and resistance possess negative values at some edges for certain values of the output impedance. Therefore, it is difficult to extract a reasonable inductivity ratio for those edges from the Kron reduced phasor model. On the contrary, the proposed inductivity measure remains within the physically valid interval $\arctan(\omega\Psi_{\text{NIR}}) \in [0, \pi/2]$. \square

Example 2 shows that θ_{NIR} can be used as a measure that estimates the phase of the lines of the overall network. A desired amount of change in this measure can be optimized by appropriate choices of output impedances. The following example illustrates this case.

Example 3 *Output impedance optimization on the IEEE 13 node test feeder.*

Figure 9 depicts the graph of the islanded IEEE 13 node

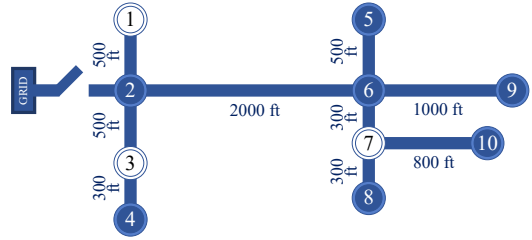


Fig. 9. Schematic of the islanded IEEE 13 node test feeder graph. Power sources are connected to the (white) nodes 1, 3, and 7.

test feeder. Here, all the distribution lines are assumed to have the same reactance per length equal to $\omega l = 1.2 \frac{\Omega}{\text{mile}}$ and resistance per length equal to $r = 0.7 \frac{\Omega}{\text{mile}}$, derived from the configuration 602 [45]. We consider the case where three inverters are connected to the nodes 1, 3, and 7, and the rest of the nodes are connected to constant current loads. After carrying out Kron reduction, the algebraic connectivity of the resulting Laplacian matrix is equal to 3.1. Before adding the output inductances, θ_{NIR} is equal to $\arctan \frac{\omega l}{r} = \frac{2\pi}{3}$. Based on the results of Theorem 1, for a 10% increase in θ_{NIR} , a uniform inductor of 3.21mH should be attached to the outputs of all the sources. However, in case non-uniform output inductors are to be used, by using the result of Theorem 3, the same increase in the network inductivity ratio can be achieved (optimally) with 0.95mH, 0.95mH, and 4.35mH inductors, for the nodes 1, 3, and 7 respectively. Both cases are feasible in practice since the typical values for inverter output filter inductance and implemented output virtual inductance range from 0.5mH to 50mH [4], [7], [11], [12], [18], [46]–[48]. However, note that the total inductance used in the (optimal) non-uniform case is considerably smaller than the one used in the uniform scheme. \square

V. CONCLUSION

In this paper, the influence of the output impedance on the inductivity and resistivity of the distribution lines has been investigated. Two measures, network inductivity ratio and network resistivity ratio, were proposed and analyzed without relying on the ideal sinusoidal signals assumption (phasors). The analysis revealed the fact that the more connected the graph is, the more output impedance diffuses into the network and the larger its effect will be. We have provided examples on how the impact of inductive output impedances on the network can be maximized in specific network topologies. We compared the proposed measure to the phase angles of the lines in a phasor-based Kron reduced network. Results confirm the validity and the effectiveness of the proposed metrics. Future works include investigating analytical solutions on maximizing the network inductivity/resistivity ratios, quantifying network inductivity in the case of heterogeneous lines, and investigating, analytically, the effect of network inductivity ratio on the performance of the droop-based methods.

REFERENCES

- [1] T. Morstyn, B. Hredzak, and V. G. Agelidis, “Distributed cooperative control of microgrid storage,” *IEEE Transactions on Power Systems*, vol. 30, no. 5, pp. 2780–2789, Sept 2015.

- [2] J. M. Guerrero, L. G. De Vicuna, J. Matas, M. Castilla, and J. Miret, "Output impedance design of parallel-connected ups inverters with wireless load-sharing control," *IEEE Transactions on industrial electronics*, vol. 52, no. 4, pp. 1126–1135, 2005.
- [3] J. M. Guerrero, J. Matas, L. G. D. V. De Vicuna, M. Castilla, and J. Miret, "Wireless-control strategy for parallel operation of distributed-generation inverters," *IEEE Transactions on Industrial Electronics*, vol. 53, no. 5, pp. 1461–1470, 2006.
- [4] J. M. Guerrero, J. Matas, L. G. de Vicuna, M. Castilla, and J. Miret, "Decentralized control for parallel operation of distributed generation inverters using resistive output impedance," *IEEE Transactions on industrial electronics*, vol. 54, no. 2, pp. 994–1004, 2007.
- [5] J. M. Guerrero, J. C. Vasquez, J. Matas, M. Castilla, and L. G. de Vicuña, "Control strategy for flexible microgrid based on parallel line-interactive ups systems," *IEEE Transactions on Industrial Electronics*, vol. 56, no. 3, pp. 726–736, 2009.
- [6] J. Guerrero, P. Loh, M. Chandorkar, and T. Lee, "Advanced control architectures for intelligent microgrids - Part I: Decentralized and hierarchical control," *IEEE Transactions Industrial Electronics*, no. 99, pp. 1–1, 2013.
- [7] Y. W. Li and C. N. Kao, "An accurate power control strategy for power-electronics-interfaced distributed generation units operating in a low-voltage multibus microgrid," *IEEE Transactions on Power Electronics*, vol. 24, no. 12, pp. 2977–2988, Dec 2009.
- [8] R. Majumder, B. Chaudhuri, A. Ghosh, R. Majumder, G. Ledwich, and F. Zare, "Improvement of stability and load sharing in an autonomous microgrid using supplementary droop control loop," *IEEE Transactions on Power Systems*, vol. 25, no. 2, pp. 796–808, May 2010.
- [9] H. Mahmood, D. Michaelson, and J. Jiang, "Accurate reactive power sharing in an islanded microgrid using adaptive virtual impedances," *IEEE Transactions on Power Electronics*, vol. 30, no. 3, pp. 1605–1617, March 2015.
- [10] R. Moslemi, J. Mohammadpour, and A. Mesbahi, "A modified droop control for reactive power sharing in large microgrids with meshed topology," in *2016 American Control Conference (ACC)*, July 2016, pp. 6779–6784.
- [11] K. D. Brabandere, B. Bolsens, J. V. den Keybus, A. Woyte, J. Driesen, and R. Belmans, "A voltage and frequency droop control method for parallel inverters," *IEEE Transactions on Power Electronics*, vol. 22, no. 4, pp. 1107–1115, July 2007.
- [12] J. Matas, M. Castilla, L. G. d. Vicua, J. Miret, and J. C. Vasquez, "Virtual impedance loop for droop-controlled single-phase parallel inverters using a second-order general-integrator scheme," *IEEE Transactions on Power Electronics*, vol. 25, no. 12, pp. 2993–3002, Dec 2010.
- [13] S. J. Chiang, C. Y. Yen, and K. T. Chang, "A multimodule parallel-series-connected PWM voltage regulator," *IEEE Transactions on Industrial Electronics*, vol. 48, no. 3, pp. 506–516, Jun 2001.
- [14] M. Hamzeh, H. Karimi, and H. Mokhtari, "A new control strategy for a multi-bus mv microgrid under unbalanced conditions," *IEEE Transactions on Power Systems*, vol. 27, no. 4, pp. 2225–2232, Nov 2012.
- [15] J. Guerrero, L. Hang, and J. Uceda, "Control of distributed uninterruptible power supply systems," *Industrial Electronics, IEEE Transactions on*, vol. 55, no. 8, pp. 2845–2859, Aug 2008.
- [16] W. Yao, M. Chen, J. Matas, J. M. Guerrero, and Z. M. Qian, "Design and analysis of the droop control method for parallel inverters considering the impact of the complex impedance on the power sharing," *IEEE Transactions on Industrial Electronics*, vol. 58, no. 2, pp. 576–588, Feb 2011.
- [17] D. M. Vilathgamuwa, P. C. Loh, and Y. Li, "Protection of microgrids during utility voltage sags," *IEEE Transactions on Industrial Electronics*, vol. 53, no. 5, pp. 1427–1436, Oct 2006.
- [18] J. Kim, J. M. Guerrero, P. Rodriguez, R. Teodorescu, and K. Nam, "Mode adaptive droop control with virtual output impedances for an inverter-based flexible AC microgrid," *IEEE Transactions on Power Electronics*, vol. 26, no. 3, pp. 689–701, March 2011.
- [19] A. Teixeira, K. Paridari, H. Sandberg, and K. H. Johansson, "Voltage control for interconnected microgrids under adversarial actions," in *2015 IEEE 20th Conference on Emerging Technologies & Factory Automation (ETFA)*. IEEE, 2015, pp. 1–8.
- [20] L. L. Grigsby, *Power system stability and control*. CRC press, 2016.
- [21] M. Ceraolo and D. Poli, *Fundamentals of electric power engineering: from electromagnetics to power systems*. John Wiley & Sons, 2014.
- [22] J. J. Grainger, W. D. Stevenson, and G. W. Chang, *Power system analysis*. McGraw-Hill New York, 1994, vol. 621.
- [23] S. Y. Caliskan and P. Tabuada, "Towards kron reduction of generalized electrical networks," *Automatica*, vol. 50, no. 10, pp. 2586 – 2590, 2014.
- [24] R. A. Horn and C. R. Johnson, *Matrix Analysis*. Cambridge university press, 2012.
- [25] M. Franceschelli, A. Gasparri, A. Giua, and C. Seatzu, "Decentralized Laplacian eigenvalues estimation for networked multi-agent systems," in *Decision and Control, 2009 held jointly with the 2009 28th Chinese Control Conference. CDC/CCC 2009. Proceedings of the 48th IEEE Conference on*, Dec 2009, pp. 2717–2722.
- [26] P. D. Lorenzo and S. Barbarossa, "Distributed estimation and control of algebraic connectivity over random graphs," *IEEE Transactions on Signal Processing*, vol. 62, no. 21, pp. 5615–5628, Nov 2014.
- [27] X. Zhao, H. Zhou, D. Shi, H. Zhao, C. Jing, and C. Jones, "On-line PMU-based transmission line parameter identification," *CSEE Journal of Power and Energy Systems*, vol. 1, no. 2, pp. 68–74, June 2015.
- [28] Y. Du and Y. Liao, "On-line estimation of transmission line parameters, temperature and sag using PMU measurements," *Electric Power Systems Research*, vol. 93, pp. 39 – 45, 2012.
- [29] D. Shi, D. J. Tylavsky, K. M. Koellner, N. Logic, and D. E. Wheeler, "Transmission line parameter identification using PMU measurements," *European Transactions on Electrical Power*, vol. 21, no. 4, pp. 1574–1588, 2011.
- [30] J. M. Guerrero, J. Matas, L. G. de Vicuna, M. Castilla, and J. Miret, "Decentralized control for parallel operation of distributed generation inverters using resistive output impedance," *IEEE Transactions on Industrial Electronics*, vol. 54, no. 2, pp. 994–1004, April 2007.
- [31] L. Y. Lu and C. C. Chu, "Consensus-based droop control synthesis for multiple dics in isolated micro-grids," *IEEE Transactions on Power Systems*, vol. 30, no. 5, pp. 2243–2256, Sept 2015.
- [32] S. Y. Caliskan and P. Tabuada, "Kron reduction of power networks with lossy and dynamic transmission lines," in *2012 IEEE 51st IEEE Conference on Decision and Control (CDC)*, Dec 2012, pp. 5554–5559.
- [33] Q.-C. Zhong and T. Hornik, *Control of power inverters in renewable energy and smart grid integration*. John Wiley & Sons, 2012, vol. 97.
- [34] U. Münz and M. Metzger, "Voltage and angle stability reserve of power systems with renewable generation," *IFAC Proceedings Volumes*, vol. 47, no. 3, pp. 9075–9080, 2014.
- [35] M. Sinha, F. Dörfler, B. B. Johnson, and S. V. Dhople, "Synchronization of liénard-type oscillators in uniform electrical networks," in *American Control Conference (ACC)*, 2016. IEEE, 2016, pp. 4311–4316.
- [36] C. D. Persis and N. Monshizadeh, "Bregman storage functions for microgrid control," *IEEE Transactions on Automatic Control*, vol. 63, no. 1, pp. 53–68, Jan 2018.
- [37] R. Grone, R. Merris, and V. S. Sunder, "The laplacian spectrum of a graph," *SIAM Journal on Matrix Analysis and Applications*, vol. 11, no. 2, pp. 218–238, 1990.
- [38] B. Mohar, "Laplace eigenvalues of graphs - a survey," *Discrete Mathematics*, vol. 109, no. 13, pp. 171 – 183, 1992.
- [39] N. M. M. De Abreu, "Old and new results on algebraic connectivity of graphs," *Linear algebra and its applications*, vol. 423, no. 1, pp. 53–73, 2007.
- [40] G. Kron, *Tensor Analysis of Networks*, 1939.
- [41] A. van der Schaft, "Characterization and partial synthesis of the behavior of resistive circuits at their terminals," *Systems & Control Letters*, vol. 59, no. 7, pp. 423 – 428, 2010.
- [42] J. K. Merikoski and R. Kumar, "Inequalities for spreads of matrix sums and products," in *Applied Mathematics E-Notes*, 4:150 159, 2004.
- [43] E. I. Verriest and J. C. Willems, "The behavior of linear time invariant RLC circuits," in *49th IEEE Conference on Decision and Control (CDC)*, Dec 2010, pp. 7754–7758.
- [44] F. Dörfler and F. Bullo, "Kron reduction of graphs with applications to electrical networks," *IEEE Transactions on Circuits and Systems I: Regular Papers*, vol. 60, no. 1, pp. 150–163, Jan 2013.
- [45] Distribution System Analysis Subcommittee, "IEEE 13 Node Test Feeder," *IEEE Power Engineering Society, Power System Analysis, Computing and Economics Committee*.
- [46] J. He and Y. W. Li, "Generalized closed-loop control schemes with embedded virtual impedances for voltage source converters with LC or LCL filters," *IEEE Transactions on Power Electronics*, vol. 27, no. 4, pp. 1850–1861, April 2012.
- [47] J. M. Guerrero, J. C. Vasquez, J. Matas, L. G. de Vicuna, and M. Castilla, "Hierarchical control of droop-controlled AC and DC microgrids; a general approach toward standardization," *IEEE Transactions on Industrial Electronics*, vol. 58, no. 1, pp. 158–172, Jan 2011.
- [48] Y. A. R. I. Mohamed and E. F. El-Saadany, "Adaptive decentralized droop controller to preserve power sharing stability of paralleled inverters in distributed generation microgrids," *IEEE Transactions on Power Electronics*, vol. 23, no. 6, pp. 2806–2816, Nov 2008.